**Climate
of the Past**

Open Access

Discussions

Quantitative reconstruction of East Asian summer monsoon precipitation during the Holocene based on oxygen isotope mass-balance calculation in the East China Sea

Y. Kubota[1], R. Tada[2], and K. Kimoto[3]

[1]Department of Geology and Paleontology, National Museum of Nature and Science, 4-1-1, Amakubo, Tsukuba, Ibaraki, 305-0005, Japan
[2]Department of Earth and Planetary Science, Graduate School of Science, The University of Tokyo, 7-3-1, Hongo, Bunkyo-ku, Tokyo, 113-0033, Japan
[3]Research Institute for Global Change, Japan Agency for Marine-Earth Science and Technology, 2-15 Natsushima-cho, Yokosuka, Kanagawa, 237-0061, Japan

Correspondence to: Y. Kubota (yoshimi@kahaku.go.jp)

Discussion Paper | Discussion Paper | Discussion Paper | Discussion Paper |

CPD

10, 1447–1492, 2014

East Asian summer monsoon precipitation

Y. Kubota et al.

Title Page

Abstract | Introduction

Conclusions | References

Tables | Figures

|◀ | ▶|

◀ | ▶

Back | Close

Full Screen / Esc

Printer-friendly Version

Interactive Discussion

Abstract

The $\delta^{18}O$ of seawater ($\delta^{18}O_w$), an indirect indicator of sea surface salinity, in the northern East China Sea (ECS) was reconstructed for the last 7 kyr using paired Mg / Ca ratio and $\delta^{18}O$ of planktic foraminiferal tests. According to modern observation, interannual variations in sea surface salinity during summer in the northern part of the ECS are mainly controlled by the discharge from the Changjiang (Yangtze River), which reflects summer rainfall in the drainage area of the Changjiang. Thus, changes in the summer sea surface salinity in the northern ECS are interpreted as reflecting variations in the East Asian summer monsoon (EASM) precipitation in South China. This interpretation is confirmed by the strong relationship between salinity in the northern ECS and the discharge from the Changjiang during wet season (May–October) based on the observational salinity data from 1951 to 2000. On the other hand, it is difficult to estimate absolute salinity value in the past with high accuracy, because there are large uncertainties in salinity-$\delta^{18}O_w$ regression slope, end-member salinity, and $\delta^{18}O_w$ values. For this reason, in order to reconstruct the discharge in the past, we conducted $\delta^{18}O_w$ mass-balance calculation to estimate freshwater contribution to the surface water of the northern ECS during the Holocene. We assumed a simple mixing between two end-members: the seawater and the freshwater from the Changjiang. Temporal variations in the relative contribution of the freshwater from the Changjiang indicates that there was no long-term decreasing trend in the Changjiang freshwater discharge since the middle Holocene, but centennial to millennial scale variations were predominant. This suggests that changes in summer insolation in the Northern Hemisphere did not mainly control the changes in summer precipitation in the South China. Our results also indicate that variability of the Changjiang freshwater during the Holocene on sub-millennial timescale was much lower than interannual time scale, but similar to decadal time scale.

1 Introduction

The East Asian summer monsoon (EASM) is generated by land-ocean thermal contrast between Asia and northwestern Pacific. The EASM is normally referred to as a sub-tropical monsoon encompassing the East Asia including eastern China, Japan, Korea and adjacent marginal seas (Zhang et al., 1996). In paleo-monosoon studies, high-resolution records of oxygen isotope composition of speleothems ($\delta^{18}O_{sp}$) from Chinese caves have been receiving wide attention (e.g., Wang et al., 2001), because the stalagmites can provide long and high resolution $\delta^{18}O_{sp}$ data, and their age models, which are based on the Uranium series datings, are of high precision and high resolution. The records of $\delta^{18}O_{sp}$ have been regarded as a proxy of the EASM precipitation or intensity (e.g., Wang et al., 2001, 2005; Yuan et al., 2004; Dykoski et al., 2005; Cheng et al., 2009), indicating that orbital-scale variations in $\delta^{18}O_{sp}$ follow the summer insolation curve of the Northern Hemisphere without any obvious time lag (0.77 ± 0.45 kyrs, Wang et al., 2008). Based on these results, the concept that intensity of the EASM is strongly influenced by the local summer insolation on orbital timescale has been accepted (e.g., Chen et al., 2012). During the Holocene, $\delta^{18}O_{sp}$ systematically increased by ∼ 2.5‰ from the middle Holocene to the late Holocene, which is interpreted as reflecting the decrease in the precipitation of the EASM in response to the decrease in summer insolation (Wang et al., 2001). Recently, however, modern data analogues (Maher and Thompson, 2012) and modeling (Pausata et al., 2011) approaches suggested that the $\delta^{18}O_{sp}$ of the Chinese stalagmites might reflect not the precipitation amount (amount effect) but other climate factors such as the moisture source itself and/or conditions in the moisture source. LeGrande and Schmidt (2009) pointed out that water isotopes were better interpreted in terms of regional hydrological cycle changes rather than as indicators of local climate based on a modeling result. Clemens et al. (2010) argued that winter temperature change impacted on $\delta^{18}O_{sp}$ (meteorological precipitation under cold conditions) and the $\delta^{18}O_{sp}$ records cannot be interpreted as reflecting the EASM signal alone. Maher and Thompson (2012) revisited the interpretation of $\delta^{18}O_{sp}$

using mass-balance calculations and argued that the $\delta^{18}O_{sp}$ variations in Chinese caves could not be accounted for by summer rainfall changes, rainfall seasonality, or winter cooling, but instead reflected changes in the moisture source, i.e., Indian Ocean or Pacific. Besides, precipitation/evaporation ratio deduced from compiled lake level records within Changjiang (Yangtze River) Basin in South China showed no decreasing trend or even slight increase from early-middle to late Holocene (An et al., 2000), which is inconsistent with the classical interpretation of $\delta^{18}O_{sp}$.

Kubota et al. (2010) reported millennial-scale variations in water properties between warm and saline Kuroshio Water and cool and less saline Changjiang Diluted Water (CDW) during the Holocene based on Mg/Ca and $\delta^{18}O$ of the planktic foraminifera, *Globigerinoides ruber*, at site KY07-04-01 (hereafter site KY), and claimed that events of higher (lower) contribution of the CDW corresponded to higher (lower) precipitation in South China and, hence, associated larger (smaller) discharge of the Changjiang freshwater. However, Kubota et al. (2010) merely reconstructed the variations in relative contribution of the two water masses, and how much of the summer precipitation (or Changjiang discharge) changed still remains to be revealed. Thus, in this study, in order to conduct the quantitative reconstruction of the Changjiang discharge, first, we calculated relative contribution of the Changjiang freshwater (f_{CFW}) to the surface water at site KY in the northern ECS during the time from middle to late Holocene. In this process, temporal changes in end-member $\delta^{18}O_w$ of the water masses that probably affects the $\delta^{18}O_w$ values at the core site were taken into consideration. Second, we estimated the flux of the freshwater from the Changjiang (volume per second; Q_{CFW}) into the ECS for the same period by applying modern empirical relationship between f_{CFW} and Q_{CFW} around the core site. Finally, we examined variability of the freshwater discharge. Centennial to millennial-scale changes in the reconstructed Q_{CFW} were compared with modern interannual and decadal changes in freshwater discharge in terms of their amplitude and duration to evaluate the variability in precipitation of the EASM in the catchment area of the Changjiang. In addition to the data published in Kubota et al. (2010), sixty-seven samples from the Holocene part of KY core were

analyzed for both Mg / Ca and $\delta^{18}O_c$ to improve the reliability of the events suggested by Kubota et al. (2010).

2 Oceanographic and climatological settings

The Changjiang is more than 6300 km in length and has a catchment area of 1.94×10^6 km^2, and its huge drainage basin covers the major part of South China (Fig. 1). The annual runoff of the Changjiang is attributed mainly to the rainfall in summer, not snowfall in winter (Chen et al., 1994). The year-to-year runoff of the Changjiang at Datong station, seaward-most hydrological station 600 km to the west from the Changjiang river mouth, is correlated with basin-wide precipitation ($R^2 = 0.81$, Xu et al., 2010), but monthly runoff lags behind average precipitation by ~ 1 month (Jiang et al., 2007). Annual runoff at Datong is approximately 8900×10^8 m^3 (2.8×10^{-2} Sv; Sv $= 10^6$ m^3 s^{-1}) in average from 1961–2000 (CWRC, 2002). The Changjiang discharge shows a remarkable seasonal cycle with the maximum in July and the minimum in January. Average water discharge during wet season (May–October) is 4.0×10^{-2} Sv at Datong, which accounts for approximately 70 % of annual total discharge (Jiang et al., 2007). The maximum and minimum discharges during wet season were observed in 1954 (6.3×10^{-2} Sv = 160 % of average value in the past ~ 50 years) and 1972 (2.8×10^{-2} Sv = 70 % of average value), respectively, during the time period from 1951 to 2000 (Fig. 2). Due to the lower discharge in dry season (November to April), interannual amplitude of the variation in annual discharge is smaller than that of the wet season.

The Changjiang supplies the huge amount of the fresh water into the northern ECS. The ECS is a marginal sea bounded by the Asian continent to the northwest, Taiwan Island to the southwest, the Ryukyu Islands to the southeast, and Kyushu and the Korean peninsula to the northeast, respectively (Fig. 3). The continental shelf shallower than 200 m occupies more than 70 % of the entire East China Sea. The Okinawa Trough, of which maximum water depth is greater than 2000 m, stretches from the southwestern

to northeastern part of the ECS along the Ryukyu Arc. The ECS connects to surrounding seas through narrow straits or gaps. The waters from the Pacific and South China Sea flow into the ECS through the Yonaguni gap and Taiwan Strait, respectively (Fig. 3). The sill depth of the Tsushima Strait and Taiwan Strait are ~ 130 and $\sim 60\,\mathrm{m}$, respectively, and that of Yonagini gap is deeper than 1000 m.

The discharge of the Changjiang accounts for $\sim 90\,\%$ of the total river discharge to the ECS (Isobe et al., 2002), and sea surface salinity (SSS) in the East China Sea changes drastically through a year due to the significant influence of the Changjiang discharge caused by the EASM precipitation. The influence of the Changjiang on the ECS is larger than the local rainfall over the ECS (Chen et al., 1994), as is also supported by the simulation result of Delcroix and Murtugudde (2002). The discharge, which empties into the Changjiang estuary, forms a water mass called Changjiang Diluted Water (CDW) by mixing with saline ambient water (e.g., Ichikawa and Beardsley, 2002). The structure and pathway of the CDW in the Chinese coastal area change seasonally. During winter, the CDW flows southward along the Chinese coast. During summer, it has a bimodal structure consisting of a southward coastal jet and a northeastward spread, and the latter eventually reaches the Japan Sea (Mao et al., 1964; Beardsley et al., 1985; Ichikawa and Beardsley, 2002). Simulations by a numerical model show that the southerly wind, which is predominant in the summer season, enhances the eastward extension of the CDW, suggesting the importance of the monsoonal wind effect on the behavior of the CDW (Lie et al., 2003). Overall, ocean currents on the East China Sea shelf are directed northeastward with a speed of an order of $10\,\mathrm{cm\,s^{-1}}$ (Fang et al., 1991; Katoh et al., 2000), meaning that the CDW takes 2–3 months to cross the shelf (roughly 700 km) from the mouth of the Changjiang to the Tsushima Strait during summer (Isobe and Matsuno, 2008). The CDW, whose thickness during summer is usually 10 to 30 m in the mid-shelf area (Lie et al., 2003; Isobe and Matsuno, 2008), is characterized by lower salinity and lower temperature compared to the Kuroshio Surface Water. The vertical advection of the cold bottom water that is remnant winter water over the shelf or from the upwelled Kuroshio subsurface

water is involved in formation of CDW during summer (Wang and Chen, 1998). Nearly, all of the river discharge during summer into the ECS flows into the Japan Sea, as contribution of the river freshwater transport leaking to the North Pacific was estimated to be small (Isobe et al., 2002).

3   Material and methods

A core material of KY07-04-01 (31°38.35′ N, 128°56.64′ E, 758 m water depth), which was retrieved from the Danjo Basin, northern edge of the Okinawa Trough (Kubota et al., 2010) was used for Mg/Ca and δ^{18}O analyses of planktic foraminifera. It is confirmed that CDW can reach to the core site across the shelf break during summer based on ^{226}Ra and ^{228}Ra measurement (Inoue et al., 2012). Inoue et al. (2012) also calculated the relative contribution of the Changjiang freshwater in this area as approximately 2–3 % in July and October using salinity and ^{228}Ra concentration data from 2008 to 2010. Based on numerous CTD observations, the maximum Sea surface temperature (SST) near the core site is 28.4 °C in August, and the minimum is 17.7 °C in February (Japan Oceanographic Data Center; available at http://www.jodc.go.jp/index_j.html). On the other hand, sea surface salinity (SSS) reaches the maximum at 34.7 PSU in February, decreases to the minimum at 33.0 PSU in July (Fig. 4). Lower salinity during summer indicates that river runoff due to the EASM dominates over the seasonal changes in the Kuroshio which works for increasing salinity during summer when its volume transport is the largest. As is shown in Fig. 4, spatial patterns of SST and SSS during summer are characterized by lower-SST and -SSS in the northwest part and higher-SST and -SSS in the southeast part of the ECS. The Kuroshio Current penetrates the ECS and flows along the shelf break from southwest to northeast throughout a year and has a major impact on SSS in the Okinawa Trough area, but its impact is confined to the southern ECS along the main Kuroshio axis in Fig. 4.

Full Screen / Esc

Printer-friendly Version

Interactive Discussion

The age model of core KY was established based on planktic foraminiferal [14]C (fourteen horizons) and the K-Ah ash layer, which was described in detail in Kubota et al. (2010). For isotopes and trace element analyses, approximately thirty to forty individual *G. ruber* were picked and those tests were crashed to homogenize. After cleaned by milli-Q water and methanol, approximately 50–70 µg of foraminiferal tests were separated and used for the oxygen isotope analysis. The δ^{18}O of *G. ruber* ($\delta^{18}O_{pf}$) was measured by a Finnigan-MAT-252 mass spectrometer (IR-MS) with Kiel III carbonate Device at Mutsu Institute for Oceanography, Japan Agency of Marine and Science and Technology (JAMSTEC) and University of Tokyo. The $\delta^{18}O_{c}$ value was determined by analysis of carbon dioxide generated from foraminiferal tests by reaction with 100 % phosphoric acid at 70° and introduced to the mass spectrometer. The reproducibility of the measurement is better than ±0.05 ‰ (1σ) for δ^{18}O and δ^{13}C as determined by replicate measurements of international standards NBS-19 (RM8544 Limestone).

After the tests were cleaned with "reductive" cleaning protocols for Mg / Ca analysis (Boyle and Keigwin, 1985), Mg / Ca analysis was performed by Finnigan ELEMENT-2 multi-sector inductively coupled plasma mass spectrometer (HR-ICP-MS) at Mutsu Institute for Oceanography, JAMSTEC. Isotopes of three elements (^{24}Mg, ^{44}Ca, ^{48}Ca, ^{55}Mn) were analyzed using Sc as the internal standard (Uchida et al., 2008). Four working standards were prepared by successive dilutions of the stock standard solutions to match the concentrations of Ca (20 ppb, 100 ppb, 500 ppb, 2 ppm) and Mg (0.05 ppb, 0.2 ppb, 1.0 ppb, 5 ppb) covering ranges of the Ca and Mg concentrations of all samples. The Milli-Q water in our laboratory was shown to have blank concentrations of much below the lowest concentration of the standard solution (e.g., 0.05 ppb for Mg) for the elements studied (Mg, Ca, and Mn).

The precision of replicate analysis of the working standard for Mg / Ca is better than ±0.09 mmol mol^{-1}, corresponding to ±0.3 °C in temperature scale. As reported by Barker et al. (2003), samples cleaned by the reductive cleaning method of Boyle and Keigwin (1985) gave lower values of Mg / Ca (by average approximately 10–15 %) than

those cleaned by the oxidative cleaning procedure of Elderfield and Ganssen (2000). Most of the samples of the core KY were cleaned by reductive methods but thirty-eight samples in Holocene section are cleaned by oxidative methods (Kubota et al., 2010). To verify difference of Mg/Ca values between reductive and oxidative cleaning methods in core KY, fifteen randomly selected samples were re-picked and cleaned with both cleaning methods. The results indicated that Mg/Ca values with oxidative cleaning methods showed 0.73 °C, on average, higher values than those with reductive cleaning methods in temperature scale. Thus, in this study, the SST values derived from Mg/Ca values with oxidative methods were subtracted 0.73 °C. Detailed discussions are described in Supplement.

The calcification depth of *G. ruber* is estimated to be upper 30 m of the water column based on the study of δ^{18}O from surface and downcore sediment samples from the South China Sea (Wang, 2000). A plankton tow observation has shown that *G. ruber* was abundant during summer in vicinity of the core site in the northern ECS, which probably responded to arrival of nutrient rich (also less saline) CDW (Yamasaki et al., 2010). Thus, this species is suitable to reconstruct the summer freshwater discharge in the past. The surface salinity around the core site begins to decrease in June associated with the arrival of CDW, but the contribution of CDW is mostly dispersed in November. Here, the calcification season of *G. ruber* is considered to be June through October. As is explained later, this assumption is reasonable based on the temperature estimate of a core top sample.

4 Results

4.1 Mg/Ca-SST

Mg/Ca analysis of *G. ruber* was carried out for core KY with approximately every 2.5–5 cm (equivalent to approximately 60 years) intervals for the time interval from 11.6 ka to the present. The measured Mg/Ca values were converted to SST using an equation

developed for *G. ruber* in the South China Sea (Hastings et al., 2001). When using this equation, the core top sample of a pilot core of site KY yields a temperature of 25.4 °C, which is close to the modern seasonally-averaged temperature through June to October at the depth ranging between surface and 30 m near the core site (=25.7 °C) (the seasonally-averaged temperature data are statistically processed by Japan Oceanographic Data Center (JODC) based on observational data from 1906 to 2003, which are available at the website http://www.jodc.go.jp/index_j.html). For core KY core, the effect of preferential removal of Mg^{2+} from foraminiferal calcite on Mg/Ca values due to dissolution on the seafloor (e.g., Dekens et al., 2002 and reference therein) is considered as negligible because the water depth of the core site (758 m) is well above the modern lysocline (approximately 1600 m) in the ECS. Even if a Mg/Ca calibration with correction for dissolution effect for Pacific (Dekens et al., 2002) is applied to Mg/Ca values of the core top sample, the corrected temperature of 25.6 °C makes only 0.2 °C difference from the non-corrected temperature. Thus, temperature errors derived from Mg/Ca calibration is smaller than the errors that stemmed from heterogeneity of samples that is ±0.45 °C.

Temporal variations of Mg/Ca-derived SST during the Holocene are shown in Fig. 5. During the early Holocene from 11.6 to 10 ka, SST increased from 24 to 26.5 °C with high frequency variations with the amplitude of ~2 °C. On the other hand, average SSTs in every 2 kyr from 10 to 0 ka mark constant values of 25.6 ~ 25.7 °C. Thus there is no long-term SST trend after 10 ka, whereas multi-centennial to millennial-scale variations are clearly observed in the SST record. Cool SST events, which were defined as intervals cooler than the average value by more than 1σ error (0.45 °C) in 5-points weighted averaged data set(= 100–400 yr average), were recognized at 8.7, 8.2, 7.1–7.0, 6.1–6.0, 4.6–4.8, 3.6–3.5, 3.2, 2.8–3.2, 1.6, and 0.5 ka, while SST events warmer than the average value by more than 1σ error were recognized at 9.9, 9.7–9.6, 9.4, 9.0, 8.0–7.9, 6.7, 6.5, 4.9–5.1, 4.5–4.1, 3.8, and 0.8–0.7 ka. The timings of these events were the same as those reported by Kubota et al. (2010). Age uncertainties (2σ) of these events were less than 250 years. This result confirmed that durations of cooler

Discussion Paper | Discussion Paper | Discussion Paper | Discussion Paper |

CPD

10, 1447–1492, 2014

East Asian summer monsoon precipitation

Y. Kubota et al.

Title Page

Abstract | Introduction

Conclusions | References

Tables | Figures

|◄ | ►|

◄ | ►

Back | Close

Full Screen / Esc

Printer-friendly Version

Interactive Discussion

or warmer events were shorter than 0.5 kyr, and especially short during the interval from 11.6 to 10 ka. Whereas the amplitudes of the multi-centennial to millennial-scale variations were larger during the interval from 5 to 3 ka.

4.2 Calculation of oxygen isotope ratio of seawater in the northern ECS

Oxygen isotope ratios of ambient seawater ($\delta^{18}O_w$) values (Fig. 5c) were calculated from $\delta^{18}O$ of planktic foraminifera *G. ruber* (Fig. 5b) using the $\delta^{18}O$–temperature relationship (Eq. 1) for benthic foraminifera reported by Shackleton (1974).

$$T = 16.9 - 4.38(\delta^{18}O_c - \delta^{18}O_w) + 0.10(\delta^{18}O_c - \delta^{18}O_w)^2 \tag{1}$$

During the Holocene, amplitudes of multi-centennial to millennial-scale oscillations of $\delta^{18}O_w$ were much larger (approximately 0.6 ‰ at the maximum in 5-points weighted-mean curve of Fig. 5c) than the amplitude of long-term decrease in $\delta^{18}O_w$ from the early Holocene to present (~ 0.26 ‰). The $\delta^{18}O_w$ values are affected by both global and regional factors. As the global sea-level continued to rise until ~ 6 ka, our $\delta^{18}O_w$ data set contains the global signal until then. When the global ice volume effect is subtracted from $\delta^{18}O_w$ of core KY using mean ocean $\delta^{18}O_w$ curve of Waelbroeck et al. (2002), heavier $\delta^{18}O_w$ events deviating by more than 1 σ (± 0.14 ‰) from the average value were recognized at 9.3–9.4, 8.4–8.3, 7.7–7.8, 6.3, 6.1, 5.7–6.0, 4.3, 2.2, 0.7–0.8, and 0.6 ka, while lighter events deviating by more than 1 σ from the average were recognized at 9.9, 9.6, 8.8–8.7, 7.0, 4.8, 2.7–3.2, and 2.4–2.3 ka. The heavier events at 9.4, 4.3, and 0.8–0.7 ka coincided with warmer SST events described in the previous subsection, and lighter events at 8.7, 7.0, 4.8, and 2.7–3.2 ka coincided with cooler SST events. Basically, heavier $\delta^{18}O_w$ events tend to coincide with warmer SST peaks, while lighter $\delta^{18}O_w$ events tend to coincide with cooler SST peaks on multi-centennial to millennial timescale confirming the observation by Kubota et al. (2010).

4.3 Estimation of relative contribution of freshwater in the northern East China Sea deduced from $\delta^{18}O_w$

In the modern ocean, $\delta^{18}O_w$ of the surface water tracks regional freshwater balance and water mass exchange (e.g., Jacobs et al., 1985). In most oceans, strong correlation between $\delta^{18}O_w$ and salinity is observed. However, the relationship between $\delta^{18}O_w$ and salinity is restricted in regional scale because of changes in associated water masses and their end-member $\delta^{18}O_w$ values. Modeling studies involving water isotope ($\delta^{18}O$ and δD) tracers in global scale hydrological cycle pointed out that changes in end-member $\delta^{18}O_w$ values should be taken into account to reconstruct past mixing ratio of the water mass (Schmidt et al., 2007; Legrande and Schmidt, 2009). For instance, results of the simulations of the water isotope ($\delta^{18}O$ and δD) tracers in hydrological cycle at 9, 6, and 3 ka using a coupled ocean-atmosphere model suggest that neither $\delta^{18}O_w$ of precipitation in the Asian region nor the slope of $\delta^{18}O_w$ to salinity in various regions including the ECS and the western tropical Pacific is constant for each time slice, which caused significant error in paleo-salinity reconstruction (LeGrande and Schmidt, 2009). For example, in the ECS, 1 ‰ decease in $\delta^{18}O_w$ of freshwater end-member causes 5 PSU underestimate of salinity when the $\delta^{18}O_w$ – salinity slope is kept at 0.2 ‰/PSU. Although precise reconstruction of the absolute salinity value of the past is difficult, it is possible to estimate the flux of the freshwater by a mass-balance calculation using $\delta^{18}O_w$ of the end-member water masses instead of converting to the salinities, especially in semi-closed marginal seas such as the ECS.

In modern ECS, four water masses, the Kuroshio Surface Water (KSW), the Kuroshio Subsurface Water (KSSW), the Changjiang Diluted Water (CDW) and the Taiwan Strait Warm Water (TSW) are prominent (Zhang et al., 2007 and reference there in). KSW and KSSW originate from the Kuroshio Current, and TSW comes from the South China Sea through the Taiwan Strait. The characteristic hydrographic variables, temperatures and salinities, of those four water bodies are listed in Table 1 for comparison. Here, the Changjiang freshwater (CFW) is used instead of the CDW for $\delta^{18}O_w$ balance

calculation at site KY. Then, the $\delta^{18}O_w$ of the surface water at site KY ($\delta^{18}O_{KY}$) can be explained by the mixing of the $\delta^{18}O_w$ including precipitation and evaporation in the ECS as expressed as follows.

$$\delta^{18}O_{CFW} * f_{CFW} + \delta^{18}O_{KSW} * f_{KSW} + \delta^{18}O_{KSSW} * f_{KSSW} + \delta^{18}O_{TSW} * f_{TSW}$$
$$+ \delta^{18}O_P * f_P - \delta^{18}O_E * f_E = \delta^{18}O_{KY} \tag{2}$$

$$f_{CFW} + f_{KSW} + f_{KSSW} + f_{TSW} + f_P - f_E = 1 \tag{3}$$

where f denotes relative contribution of each water mass. Subscripts CFW, KSW, KSSW, TSW, P, E, and KY denote the Changjiang freshwater, the Kuroshio Surface Water, the Kuroshio Subsurface Water, the Taiwan Strait Water, precipitation and evaporation over the ECS, and site KY, respectively.

First, consider the effect of the precipitation and evaporation in Eq. (2). At present, precipitation over the entire ECS is 1.9×10^{-2} Sv from June to October, while evaporation is 1.2×10^{-2} Sv during the same season (Chen et al., 1994). Modern $\delta^{18}O_P$ field in the East China Sea ranges from -6 to $-10‰$ based on Global Network of Isotopes in Precipitation (GNIP) observations (IAEA, 2001). $\delta^{18}O_E$ is estimated to be -6 to $-11‰$ for the range of the $\delta^{18}O_P = -6$ to $-10‰$ based on mass-balance consideration using Eqs. (2) and (3). Thus, $\delta^{18}O_P$ and $\delta^{18}O_E$ can be mostly canceled out each other. Considering much smaller contribution of the net precipitation flux ($f_P - f_E < 0.5\%$), the impact of these terms on $\delta^{18}O_{KY}$ in Eq. (3) can be negligible (($\delta^{18}O_P * f_P - \delta^{18}O_E * f_E$) < 0.05‰).

For further simplifying the Eqs. (2) and (3), we assumed a simple water mixing between the freshwater and seawater in the ECS as follows. KSW, KSSW, and TSW were treated together as the one end-ember, and called Kuroshio and Taiwan Strait Water (KTW = KSW + KSSW + TSW) in this study. In fact, modern values of $\delta^{18}O_{KSW}, \delta^{18}O_{KSSW}$, and $\delta^{18}O_{TSW}$ are all within approximately $0.2 \pm 0.09‰$, hence,

those three water masses can be treated as a single end-member compared with extremely light $\delta^{18}O_{CFW}$ (approximately $-7\,‰$) (Table 1). KSW and KSSW flow into the ECS shelf through the northeast of Taiwan (Isobe, 2008), and except that, it is assumed that there is no other intrusion of the Kuroshio waters entering the shelf of the ECS. TSW enters the ECS through the Taiwan Strait. The freshwater (CFW) as the other end-member increases its salinity by mixing with KTW while traveling northeastward on the shelf, reaches to site KY.

Based on the direct measurement of the flow speeds in the Taiwan Strait, the flux of TSW Q_{TSW} ($Sv = 10^6\,m^3\,s^{-1}$) was reported to be $1.4\,Sv$ during summer (Isobe, 2008). In contrast, the flux of the KSW (Q_{KSW}) and KSSW (Q_{KSSW}) can be estimated to be $1.2\,Sv$ by the difference in the water flux between the Taiwan Strait ($1.2\,Sv$) and the Tsushima Strait ($2.6\,Sv$) as the connectivity of the volume transports between the Taiwan and the Tsushima Straits can be assumed (Isobe, 2008). Thus, $Q_{TSW}:(Q_{KSW} + Q_{KSSW})$ is close to 1:1 during summer. A proportion of KSW and KSSW that move onto the shelf is referred to Chen and Wang (1999): $Q_{KSW} : Q_{KSSW} \sim 1:1$. Finally, the following proportion is obtained: $Q_{TSW} = 2Q_{KSW} = 2Q_{KSSW}$.

Thus, changes in $\delta^{18}O_w$ at KY site ($\delta^{18}O_{KY}$) can be explained by mixing of the two end-member $\delta^{18}O_w$ with CFW as one and KTW as the other as follows.

$$\delta^{18}O_{CFW} * f_{CFW} + \delta^{18}O_{KTW} * f_{KTW} = \delta^{18}O_{KY} \tag{4}$$

$$f_{CFW} + f_{KTW} = 1 \tag{5}$$

Subscript KTW denote Kuroshio and Taiwan Strait Water (=KSW + KSSW + TSW).

4.3.1 Reconstruction of temporal changes in $\delta^{18}O_W$ of end member of the Kuroshio and Taiwan Strait Water (KTW)

In the southern ECS, three data sets of SST and $\delta^{18}O_w$, which were calculated from Mg / Ca and $\delta^{18}O$ of *G. ruber*, are available for the end-member of KSW from cores

MD012403 (hereafter 2403) (25°04′12″ N, 123°16′48″ E, water depth of 1420 m: Lin et al., 2006), MD012404 (hereafter 2404) (26°38′50″ N, 125°48′45″ E, water depth of 1397 m: Chen et al., 2010), and A7 (126°59′ E, 27°49′ N, water depth of 1264 m: Sun et al., 2005) (Fig. 4). All of these sites are located under the main path of the Kuroshio Current. Using the same equation (Hastings et al., 2001) to convert Mg/Ca to SST, core top measurements of Mg/Ca at 2403 and A7 yielded 27.6 and 26.6 °C, respectively, that are close to the present-day average temperature during summer (June to October) with depth from the surface to 30 m at each site (Lin et al., 2006; Sun et al., 2005). Although, SST of the core top sample at 2404 is not presented, average SST from 2 to 0 ka is consistent with modern summer temperature at 2404 site. These evidences indicate that SSTs from 2403, 2404, and A7 cores reflect the season and depth that are comparable to those at KY site.

Temporal changes in SST and $\delta^{18}O_w$ at sites 2403, 2404, A7, and KY during the Holocene are shown in Fig. 6. Age models of these cores were established by ^{14}C of planktic foraminifers with high enough time resolution (every $\sim$ 1–2 kyrs). The temporal changes in SSTs at sites 2403 and 2404 showed temperatures approximately 2 °C higher than that of KY site during the early Holocene, and keep these differences throughout the entire Holocene (Fig. 6a). Approximately 2 °C difference in SST between the southern ECS and northern ECS (KY) is seen in modern SST distribution (Fig. 4).

All of $\delta^{18}O_w$ averaged in the late Holocene (2–0 ka) in 2403, 2404, and A7 sites also showed values approximately 0.2 ‰ higher than those at KY site (Fig. 6b). The 0.2 ‰ higher in $\delta^{18}O_w$ corresponds to 1 PSU higher value in salinity scale (0.2 ‰/PSU, Oba, 1990). Although 1 PSU difference is approximately 0.5 PSU larger than the value expected from modern distribution of salinity during summer (Fig. 4), 0.5 PSU (0.1 ‰) difference is within the error of $\delta^{18}O_w$ propagated from Mg/Ca-SST and $\delta^{18}O_{pf}$. There were approximately 0.4 ‰ decreasing trend in all of the $\delta^{18}O_w$ records of sites 2403, 2404, and A7 from the early to middle Holocene. This trend is mostly attributed to the retreat of the continental ice.

According to Zhang et al. (2007), any of SSTs and $\delta^{18}O_w$ at sites 2403, 2404, and A7 could be used as those of the KSW end-member based on the modern observation. However, on millennial-scale, timing and amplitude of $\delta^{18}O_w$ changes at these three sites do not seem to be similar even if the age uncertainties are taken into consideration. This is possibly due to large analytical error, local variability of precipitation/evaporation, or large error in $\delta^{18}O_w$ attributable to heterogeneity of the samples. In order to obtain the end-member $\delta^{18}O_w$ of the KSW and its temporal changes, the original $\delta^{18}O_w$ data from sites 2404, 2403, and A7 were smoothed by 5-points weighted-mean, respectively, and then $\delta^{18}O_w$ values of every 100 year interval were resampled from the each weighted-mean $\delta^{18}O_w$ data for the time interval from 11.6 to present using the software "*Analyseries*" (http://www.lsce.ipsl.fr/logiciels/index.php). Then, the evenly spaced data set with 100-year interval for sites 2404, 2403, and A7 were averaged. Because $\delta^{18}O_w$ data for KSSW during the last 7 kyr is not currently available, the end-member $\delta^{18}O_w$ of the KSSW was created hypothetically by adding 0.05‰ to $\delta^{18}O_w$ of the KSW, which was the difference between $\delta^{18}O_w$ of the KSSW and KSW observed at present (Table 1).

The SST and $\delta^{18}O_w$ data in the northern South China Sea (MD05-2904, hereafter 2904, 19°27′19″ N; 116°15′09″ E; water depth of 2066 m; Steinke et al., 2011) during the Holocene, which was also derived from paired measurement of Mg/Ca and $\delta^{18}O$ of *G. ruber* and, have been recently published (Fig. 6). The data set was calculated using the same equations used for core KY and other three sites from the ECS. The site 2904 is situated in the northern South China Sea, relatively close to the Taiwan Strait. *G. ruber* is also abundant during warmer months in the South China Sea (Lin et al., 2004). A core top Mg/Ca-SST at site 2904 in the northern South China Sea was 27.4 °C, which was only 0.5 °C cooler than the average SST during summer (June–October) at present. The average SSS of the TSW from June–October is 33.94 PSU. Although there is no $\delta^{18}O_w$ data obtained from the core top for site 2904, average $\delta^{18}O_w$ (2–0 ka) of core 2904 yields a reasonable value (−0.18‰) to the one derived

from modern SSS-$\delta^{18}O_w$ relationship in the South China Sea ($\delta^{18}O_w$ = 0.207*SSS–6.65; Shimamura et al., 2005). Thus, time-series of $\delta^{18}O_w$ record of site 2904 can be used as $\delta^{18}O_w$ of end-member of TSW.

An age model of the core 2904 was established based on two control points of cal-ibrated ^{14}C ages (Ge et al., 2010). The time-series $\delta^{18}O_w$ of site 2904 was variable, and showed large amplitude during the interval from $\sim$ 10 to $\sim$ 6 ka (Fig. 6). A temporal heavier shift in $\delta^{18}O_w$ record from site 2904 at $\sim$ 6 ka corresponded to heavier $\delta^{18}O_w$ values of site KY around 6 ka, suggesting that the changes in $\delta^{18}O_w$ end-member of the TWS might have influenced on $\delta^{18}O_w$ of site KY at least in part. 5-point weighted-mean $\delta^{18}O_w$ data set was created from original $\delta^{18}O_w$ data of site 2904 and resampled at every 100 year interval as was done for the southern ECS sites.

Eventually, the temporal variations in end-member $\delta^{18}O_w$ of the KTW was ob-tained by averaging all of the seawater mass end-member data set for $\delta^{18}O_w$ of the KSW, KSSW, and TSW with their proportions of $Q_{TSW} = 2Q_{KSW} = 2Q_{KSSW}$ ($\delta^{18}O_{KTW} = 1/2 \cdot \delta^{18}O_{TSW} + 1/4 \cdot (\delta^{18}O_{KSW} + 0.05)$): Fig. 7). We assumed that this pro-portion has been maintained at least since 7 ka when the sea level reached approx-imately the modern level, as the flow rate in the Taiwan Strait should be significantly affected by lowering of the sea level due to its shallow sill depth.

4.3.2 Reconstruction of temporal changes in $\delta^{18}O_W$ of the freshwater end member

In order to obtain the time-series data set of $\delta^{18}O_{CFW}$ during the Holocene, we utilized the Chinese speleothem $\delta^{18}O$ because $\delta^{18}O$ of the rainfall can be calculated using calcite equilibrium equation (O'Neil et al., 1969; expressed as Eq. (1).

For the Holocene, four data set of speleothem $\delta^{18}O$ from three caves are cur-rently available in the Changjiang catchment area. Among these data, we choose the speleothem $\delta^{18}O$ from Heshang Cave, which is located in Qingjiang Valley of the mid-dle reaches of the Changjiang (30°27′ N, 110°25′ E; 294 m elevation). As the summer

monsoon with its abundant precipitation results in isotopic signatures that are closer to the values typically observed in summer precipitation of the lower and middle reaches (Muller et al., 2012), precipitation δ^{18}O at Heshang Cave can be regarded as reflecting average value of the precipitation δ^{18}O within the catchment of the Changjiang. The geological and climatological settings around this cave are well studied and drip water δ^{18}O in this cave responds rapidly (less than 1 month lag) to the changes in rainfall δ^{18}O (Johnson et al., 2006). The mean annual precipitation is 1460 mm, with approximately 80 % of the annual rainfall occurring during the summer monsoon months of June-August (Johnson et al., 2006). Since the summer precipitation amount accounts for 80 % of the annual total precipitation, amount-weighted annual mean drip-water δ^{18}O (−7.4‰) at this cave site (Johnson et al., 2006) shows the value similar to the average δ^{18}O of rainfall from June to August, −7.8‰. Also, the drip-water δ^{18}O (−7.4‰) is close to modern wet season (May to October) $\delta^{18}O_{CFW}$ at the Changjiang mouth (−7.4 to −5.8‰, Zhang et al., 1990). This is because contribution of the heavy δ^{18}O of the rainfall in other months (−5.5‰, on average) (November to April) on the annual rainfall δ^{18}O is very small. Because the recharge of the water into this cave is rapid and humidity of the cave is higher than 95 % throughout the year, evaporation does not alter the δ^{18}O of rainfall before it precipitates as stalagmites in the modern setting (Hu et al., 2008). Moreover, the speleothem calcites in this cave are considered as having been precipitated under equilibrium condition because signature of kinetic effect is lacking (Hu et al., 2008).

Because the speleothem in this cave provides a continuous $\delta^{18}O_c$ record since 9.5 ka (Hu et al., 2008), temporal changes in $\delta^{18}O_w$ of drip water can be calculated if the cave temperature is known. Johnson et al. (2006) reported annual average cave temperature of 17.1 °C at present. On the other hand, Shi et al (1993) claimed that deviations of the annual temperature from present-day values during the middle Holocene were +2 °C in the Changjiang Basin based mainly on pollen analyses. Since the annual surface air temperature is considered to have reached its maximum during the middle Holocene (Shi et al., 1993), +2 °C change must be the maximum estimate for the cave

temperature change throughout the Holocene. Although $+2\,^\circ\mathrm{C}$ increase in cave temperature leads to $\sim 0.5\,‰$ increase in estimate of drip-water $\delta^{18}O$, the impact of the temperature change of this magnitude on the estimate of f_{CFW} was less than $0.15\,\%$, hence, very small.

Assuming that the cave temperature has been constant at $17.1\,^\circ\mathrm{C}$ through the entire Holocene, temporal changes in $\delta^{18}O$ of the drip water, which is considered to have been equal to $\delta^{18}O$ of the rainfall that mainly reflects summer season, during the Holocene is presented in Fig. 7. $\delta^{18}O_{CFW}$ showed distinct long-term increasing trend $(1.5\,‰)$ since $\sim 5\,\mathrm{ka}$, whereas millennial-scale variations are less prominent. Another speleothem record from Sanbao Cave which is located in the middle reaches of the Changjiang ($31°40'$ N, $110°26'$ E, $1900\,\mathrm{m}$ above sea level) also has long-term increasing trend from middle Holocene to the present with the magnitude of approximately $-1.5\,‰$, which is similar to that of the Heshang speleothem, although absolute value in Sanbao is $\sim 1\,‰$ lighter than Heshang due to the altitude effect. Thus, the increasing trend of $1.5\,‰$ (or $1.0\,‰$ increase with $+2\,^\circ\mathrm{C}$ temperature increase) in drip-water $\delta^{18}O$ is a robust feature in the Changjiang Basin.

4.3.3 Reconstructed contribution of the Changjiang freshwater

The f_{CFW}, which was calculated by Eqs. (4) and (5), varied between 5 and $0\,\%$ on millennial–scale since $7\,\mathrm{ka}$ (Fig. 8). The decreasing trend from the middle to late Holocene, which is a characteristic feature of the Chinese speleothems' $\delta^{18}O$ records, was absent in the f_{CFW} profile. As to centennial to millennial-scale variations, higher f_{CFW} events were recognized at 7–6.5, 4.7, 5.3, and $3.0\,\mathrm{ka}$, while lower events were recognized at 8.3–7.3, 5.8–6.0, 4.3, 3.5, and $2.1\,\mathrm{ka}$. Although amplitude of these centennial to millennial-scale variations in the speleothem $\delta^{18}O$ is approximately $1\,‰$ at the maximum, $1\,‰$ difference in $\delta^{18}O_w$ freshwater end-member leads to only $0.3\,\%$ difference in f_{CFW}. Thus short-term changes in $\delta^{18}O_w$ of the freshwater end-member do not alter the reconstructed results of f_{CFW} significantly. Among the factors that would affect the results of f_{CFW}, the most significant one is Mg / Ca derived error that propagates

to the results of $\delta^{18}O_w$ for each core ($\pm 0.14\,‰$). Thus, the estimate of f_{CFW} in Fig. 8 is depicted with the consideration of $\pm 0.14\,‰$ error.

4.4 Flux estimation of the Changjiang freshwater

As the sill depth of the Taiwan Strait is shallow, the circulation regime in the ECS highly depended on the sea-level change and associated topographic change (Uehara et al., 2002; Kao et al., 2006). Thus, in this study, the reconstruction of the Changjiang freshwater flux was conducted on the time interval from 7 ka to present when the sea-level and associated geography stay relatively similar to the present, and ocean surface current in the ECS should have been more or less the same as the present (Uehara et al., 2002). In order to estimate the past flux of Changjiang freshwater (Q_{CFW}) into the ECS, modern relationship between Q_{CFW} and f_{CFW} at site KY is examined. Subsequently, the past Q_{CFW} during the Holocene is estimated using the modern Q_{CFW}versus f_{CFW} relationship at the core site. Reconstruction of the absolute salinity value is not necessary when using this method, and this method can avoid introducing additional errors caused by the process of salinity reconstruction.

For observational data, f_{CFW} in site KY can be estimated by using salinity and water mass-balance calculation described in Eqs. (6) and (7).

$$S_{KTW} * Q_{KTW} = S_{KY}(Q_{CFW} + Q_{KTW}) \tag{6}$$

$$Q_{CFW}/Q_{KTW} = f_{CFW}/f_{KTW} \tag{7}$$

where S and Q denote salinities and fluxes of each water mass, respectively. Subscripts are same as in Eq. (3).

First, for Q_{CFW}, modern observational data of the Changjiang freshwater discharge were collected for 50 years from 1951 to 2000 at Datong hydrological station during wet season (May–October) (Fang et al., 2011). Here, S was defined as the salinity averaged from June through October, taking into consideration one month for CDW to

reach site KY. For S_{KY}, the original data set of the salinity around site KY (within 1° grid box of 30–31° N and 127–128° E), which was obtained by the Nansen bottle water sampler, MBT, XBT and CTD, from 1951 to 2000 was downloaded from online archive (http://www.jodc.go.jp). Then, the original salinity data from 0 to 30 m water depth were
5 averaged for each year from July through August, because the data set is not evenly spaced with respect to season and biased toward July and August. The salinity data does not exist for 1957 and 1961. In order to adjust the data's seasonality in accordance with Q_{CFW}, 0.25 PSU, which was yielded based on monthly averaged salinity data that was processed by JODC, was added to the July-August data set for each year.

10 By contrast, a fixed value (34.38 PSU) was applied to S_{KTW}, because salinity observation is sparse both in the Taiwan Strait and the southern ECS and 50-year continuous data set does not exist. The fixed value is acceptable as the interannual changes in salinity are small in the Taiwan Strait (Kalnay et al., 1996) and the southern ECS based on standard deviation of the surface salinity data (JODC).

15 The interannual correlation between the Changjiang discharge and f_{CFW} was poor ($R^2 = 0.16$, not shown) probably due to ∼ 2–3 years residence time for the waters on the East China Sea. By contrast, a strong correlation between 5-year-mean S_{KY} and f_{CFW} was found (Fig. 9a and b). This is reasonable with respect to a flood/drought cycle that shows 5.09 year cycle for the Changjiang (Jiang et al., 2006). The 5-year-mean
20 salinity data for the period 1985–1990 was deviated from a regression line and showed lower vales than that was expected from the Changjiang discharge during this period (Fig. 9). The lower salinity water, lower than expected from the Changjiang discharge, in this period might have been attributed to (1) increase in the precipitation around the core site, (2) decrease in salinity in the Kuroshio Waters and/or TSW. Analyzing obser-
25 vational salinity data within a grid of 24–25° N, 122–123° E that was downloaded from JODC data archive, there was evidence that showed −0.3 PSU deviations from the average in 1989 and 1990 for the Kuroshio Water. Thus, it is likely that the lower salinity at site KY is attributed to the decrease in salinity of the end-member although the possibility of the increase in the local precipitation might not be ruled out. The data for

period 1996–2000 should be omitted due to a larger annual variability ($\sigma^2 = 1.72$ PSU) than other period ($\sigma^2 = 0.1$–0.2 PSU), although it was in good agreement with the regression line. Omitting the data for the periods 1985–1990 and 1996–2000, a clear positive relationship ($R^2 = 0.94$) between Q_{CFW} and f_{CFW} was obtained (Line 1: Q_{CFW} ($\times 10^{-2}$ Sv) = 0.25 f_{CFW} (%) + 3.52). Even if the data during 1985–1990 was included, a robust relationship was still yielded ($R^2 = 0.58$), but a slope of the regression line becomes smaller (Line 2: Q_{CFW} ($\times 10^{-2}$ Sv) = 0.21 f_{CFW} (%) + 3.54). Y-intercepts of both of the regression lines were not zero but pointed to 3.5 ($\times 10^{-2}$ Sv), suggesting that the discharge cannot be detected at this core site when the discharge is lower than 3.5 $\times 10^{-2}$ Sv. Because site KY is situated in the easternmost part within the northern half of the ECS where the influence of the Changjiang freshwater discharge is minimal, sensitivity of salinity to variations in the Changjiang freshwater influx at KY site is low.

The regression Line 1 was used for the calculation of the Holocene Q_{CFW} (Fig. 10a). We also conducted a calculation using the regression Line 2, but the results do not show large difference ($< 0.2 \times 10^{-2}$ Sv) from Q_{CFW} using Line 1 due to almost the same slope and y-intercept between the two lines. Along with the temporal changes in f_{CFW}, there was no long-term trend in time-series Q_{CFW} record since the middle Holocene. Average Q_{CFW} from middle through late Holocene is 4.3×10^{-2} Sv, which is close to the modern average for 1951–2000 (4.0×10^{-2} Sv). Maximum and minimum of the reconstructed Q_{CFW} with Line 1 since 7 ka are 4.9×10^{-2} Sv (122 % of present-day average) and 3.7×10^{-2} Sv (93 % of present-day average), respectively. This range is smaller than interannual variability (2.8–6.3×10^{-2} Sv), but larger than decadal variability (3.6–4.6×10^{-2} Sv) in the past 50 years from 1951 to 2000 (Figs. 2 and 10).

East Asian summer monsoon precipitation

Y. Kubota et al.

Full Screen / Esc

Printer-friendly Version

Interactive Discussion

5 Discussion

Millennial scale variations in Changjiang freshwater discharge and possible linkage to ENSO variations during the Holocene

At present, the El Niño/Southern Oscillation (ENSO) is a prominent ocean-atmosphere coupled system and has a large impact on global climate on interannual time scale (Trenberth et al., 1998). There has been documented that the ENSO extreme phases are linked with major episodes of floods and droughts in many locations worldwide (Jain and Lall, 2001; Aceituno, 1988; Amarasekera et al., 1997). The linkage of the floods/droughts with ENSO has been investigated in the EASM dominant region (e.g. Chang and King, 1999; Dilley and Heyman, 1999; Lan et al., 2002; Zhang et al., 2006). The most pronounced low-level anomalous anticyclone over the western North Pacific, persisting from the El Niño mature winter to the subsequent summer, plays a crucial role in the El Niño-EASM teleconnection (Wang et al., 2000; Chang et al., 2000; Zhou et al., 2009).

As to the Yellow River, the occurrences of El Niño are accompanied by high probability of low discharge while the occurrences of La Niña are accompanied by floods events (Lan et al., 2002). The teleconnections between flood/drought events and ENSO have been investigated also in the Changjiang (Jiang et al., 2006; Zhang et al., 2006, 2007). Jiang et al. (2006) analyzed the relationship between flood/drought events in the Changjiang Basin and ENSO events during 1868–2003 by means of χ^2 test and spectral analysis. The result suggests that ENSO events and flood/drought variations are significantly correlated at a 5.04 year period and a 10 to 12 year period. Liu et al. (2008) attempted to reveal the dynamical structure and origin of the interannual variability of the EASM and its precipitation based on modern instrumental record (1979–2006), showing that the leading mode of interannual variation (39 % of the total variance) is primary associated with decaying phase of major El Niño. Namely, when El Niño occurs, the rainfall in subsequent summer intensifies along the Changjiang Basin, while the rainfall decrease over northern China in accordance with the southwestward

displacement of the western North Pacific subtropical high (Liu et al., 2012). In short, in decaying phase of El Niño the precipitation anomaly in the following summer exhibits a "Southern (Changjiang) flood and Northern (Yellow River) drought" pattern over eastern China (Huang and Huang, 2012). While the peaks of the time evolution of the
5 leading mode are primary associated with decaying El Niño, most of the major minima in the time series of the leading mode are not associated with La Niña decaying years, suggesting that the response of the EASM leading mode to ENSO is nonlinear (Liu et al., 2012).

The modern relationship between decaying phase of El Niño/La Niña and the
10 Changjiang freshwater discharge at Datong in wet season (1950–2000) is depicted in Fig. 11. High discharge in 1998 and 1954 exceed 2σ of standard deviation of the period from 1950 to 2000 and its occurrences are followed by El Niño events. The reconstructed freshwater discharge since 7 ka show the maximum discharge was 4.9×10^{-2} Sv around 4.7 ka. The increase of 0.9×10^{-2} Sv, which is compared to mean
15 value of 4.0×10^{-2} Sv for the period from 1951–2000, is equivalent to the thirty-nine occurrence of high discharge of 1954 case (6.3×10^{-2} Sv) per 100 years if all of the increase of the discharge is attributed to extreme high discharge events. This is 13 times more frequent compared to the interval from 1900 to 2000 when the extreme high discharge events exceeding 2σ ($> 5.3 \times 10^{-2}$ Sv) occur three times per 100 years.
20 Similarly high discharge intervals occurred especially in ~ 4.7 and ~ 3.0 ka since 7 ka.

The reconstructed temporal changes in the freshwater discharge since 7 ka was compared with temporal changes in the occurrence frequency of El Niño events, which were reconstructed from color of sediment in lake Laguna Pallcacocha in the southern Ecuadorian Andes (Moy et al., 2002) in Fig. 10. The record of the El Niño events during
25 the Holocene in Ecuador reconstructed by Moy et al. (2002) was based on the observation that light-colored laminae deposited in the past 200 year generally correlated with known El Niño events in instrumental and historical records. They suggested that anomalous increase in precipitation associated with El Niño caused increases in discharge, sediment load, and finally deposition of the inorganic laminae with light color.

Figure 10 shows that episodes of the lower freshwater discharge of the Changjiang in 5.8–5.7 and 4.3–4.2 ka correspond to very low occurrence of El Niño events in Ecuador, while episodes of higher discharge of the Changjiang in 4.7–4.5, and 2.7–3.1 ka tend to correspond to frequent occurrence of El Niño events. These relationship imply that temporal increase/decreases in the Changjiang discharge in these periods is possibly associated with ENSO through displacement of western North Pacific anticyclone as inferred from interannual variations (Liu et al., 2008).

6 Summary

We estimated the relative contribution of the Changjiang freshwater in the northern ECS during the Holocene using $\delta^{18}O_w$ of the surface water and assumed a two end-member mixing model with taking into consideration of the temporal changes in end-member $\delta^{18}O_w$ of the KTW and CFW. In addition, we analyzed the instrumental salinity data in a grid of 31–32° N, 128–129° E during the past 50 years (1951–2000) and demonstrated the robust relationship between relative contribution of the Changjiang freshwater (f_{CFW}) around core site in the northern ECS and the Changjiang freshwater discharge (Q_{CFW}). Subsequently, the flux of the Changjiang freshwater during the Holocene was reconstructed using the modern empirical relationship between f_{CFW} and Q_{CFW}. The reconstructed Q_{CFW} revealed following findings.

1. There was no long-term decreasing trend in the Changjiang freshwater discharge, indicating that there was no significant change in the EASM precipitation in South China from the middle Holocene. This result suggests that temporal changes in summer precipitation in South China during the Holocene did not respond to the summer insolation changes in the Northern Hemisphere.

2. Sub-millennial to millennial-scale variations in the discharge of the Changjiang freshwater were predominant and its variability was larger than decadal scale, but much smaller than interannual scale.

Supplementary material related to this article is available online at http://www.clim-past-discuss.net/10/1447/2014/cpd-10-1447-2014-supplement.pdf.

References

Aceituno, P.: On the functioning of the Southern Oscillation in the South American sector. Part I: Surface climate, Mon. Weather Rev., 116, 505–524, 1988.

Amarasekera, K. N., Lee, R. F., Willianms, E. R., and Eltahir, E. A. B.: ENSO and the natural variability in the flow of tropical rivers, J. Hydrol., 200, 24–39, 1997.

An, Z., Porter, S. C., Kutzbach, J. E., Wu, X., Wang, S., Liu, X., Li, X., and Zhou, W.: Asynchronous Holocene optimum of the East Asian monsoon, Quat. Sci. Rev., 19, 743–762, 2000.

Beardsley, R. C., Limburber, R., Yu, H., and Cannon, G. A.: Discharge of the Changjiang (Yangtze River) into the East China Sea, Cont. Shelf Res., 4, 57–55, 1985.

Changjiang Water Resource Commission (CWRC): Floods and Droughts in the Yangtze River Catchment, Beijing, 326, 2002.

Chang, W. Y. B. and King, G.: Centennial climate changes and their global associations in the Yangtze River (Chang Jiang) Delta, China and subtropical Asia, Clim. Res., 2, 95–103, 1994.

Chen, C., Beardsley, R. C., Limburber, R., and Kim, K.: Comparison of winter and summer hydrographic observations in the Yellow and East China Seas and adjacent Kuroshio during 1986, Cont. Shelf Res., 14, 909–928, 1994.

Title Page

Abstract | Introduction

Conclusions | References

Tables | Figures

◄ | ►

◄ | ►

Back | Close

Full Screen / Esc

Printer-friendly Version

Interactive Discussion

Chen, C. T. A., Ruo, R., Pai, S. C., Liu, C. T., and Wong, G. T. F.: Exhange og water masses between the East China Sea and the Kurohsio off northern Taiwan, Cont. Shelf Res., 15, 19–39, 1995.

Chen, C. T. A. and Wang, S.-L.: Carbon, alkalinity and nutrient budget on the East China Sea continental shelf, J. Geophys. Res., 104, 20675–20686, 1999.

Cheng, H., Fleitmann, D., Edwards, R. L., Wang, X., Cruz, F. W., Auler, A. S., Mangini, A., Wang, Y., Kong, X., Burns, S. J., and Matter, A.: Timing and structure of the 8.2 kyr B.P. event inferred from 18O records of stalagmites from China, Oman, and Brazil, Geology, 37, 1007–1010, doi:10.1130/g30126a.1, 2009.

Cheng, H., Zhang, P. Z., Spötl, C., Edwards, R. L., Cai, Y. J., Zhang, D. Z., Sang, W. C., Tan, M., and An, Z. S.: The climatic cyclicity in semiarid-arid central Asia over the past 500,000 years, Geophys. Res. Lett., 39, L01705, doi:10.1029/2011gl050202, 2012.

Dansgaard, W.: Stable isotopes in precipitation, Tellus, 16, 436–468, 1964.

Dekens, P. S., Lea, D. W., Pak, D. K., and Spero, H. J.: Core top calibration of Mg / Ca in tropical foraminifera: Refining paleotemperature estimation, Geochem. Geophys. Geosyst., 3, 1–29, doi:10.1029/2001gc000200, 2002.

Delcroix, T. and Murtugudde, R.: Sea surface salinity changes in the East China Sea during 1997–2001: Influence of the Yangtze River, J. Geophys. Res., 107, 8008, doi:10.1029/2001jc000893, 2002.

Dilley, M. and Heyman, B. N.: ENSO and disaster: droughts, floods and El Nin~o/Southern Oscillation warm events, Disasters, 19, 181–193, 1995.

Dykoski, C., Edwards, R., Cheng, H., Yuan, D., Cai, Y., Zhang, M., Lin, Y., Qing, J., An, Z., and Revenaugh, J.: A high-resolution, absolute-dated Holocene and deglacial Asian monsoon record from Dongge Cave, China, Earth Planet. Sci. Lett., 233, 71–86, doi:10.1016/j.epsl.2005.01.036, 2005.

Fang, G., Zhao, B., and Zhu, Y.: Water Volume Transport Through the Taiwan Strait and the Continental Skelf of the East China Sea Measured with Current Meters, Oceanogr. Asian Marg. Seas, 54, 345–358, 1991.

Fang, J., Li, Y., Sun, Z., and Deng, J.: Analysis of Runoff Change Characteristics at Datong Station of Yangtze River, Water Resour. Power, 5, 9–12, 2011.

Hastings, D. W., Kienast, S. S., and Whitko, A. A.: A comparison of three independent paleotemperature estimates from a high resolution record of deglacial SST records in the tropical South China Sea, Eos Trans. AGU, 82, Abstract PP12B-10, 2001.

Hu, C., Henderson, G. M., Huang, J., Xie, S., Sun, Y., and Johnson, K. R.: Quantification of Holocene Asian monsoon rainfall from spatially separated cave records, Earth Planet. Sci. Lett., 266, 221–232, doi:10.1016/j.epsl.2007.10.015, 2008.

Huang, S. and Huang, F.: Spatial-temporal variations of dominant drought/flood modes and the associated atmospheric circulation and ocean events in rainy season over the east of China, J. Ocean University of China, 11, 137–146, doi:10.1007/s11802-012-1813-1, 2012.

IAEA: GNIP Maps and Animations, International Atomic Energy Agency, Vienna, available at: http://isohis.iaea.org (last access: 25 March 2014), 2001.

Ichikawa, H. and Beardsley, R. C.: The Current System in the Yellow and East China Seas, J. Oceanogr., 58, 77–92, 2002.

Inoue, M., Yoshida, K., Minakawa, M., Kiyomoto, Y., Kofuji, H., Nagao, S., Hamajima, Y., and Yamamoto, M.: Spatial variations of ^{226}Ra, ^{228}Ra, and ^{228}Th activities in seawater from the eastern East China Sea, Geochem. J., 46, 429–441, 2012.

Isobe, A.: Recent Advances in Ocean-Circulation Research on the Yellow Sea and East China Sea Shelves, J. Oceanogr., 64, 569–584, 2008.

Isobe, A., Ando, M., Watanabe, T., Senjyu, T., Sugihara, S., and Manda, A.: Freshwater and temperature transports through the Tsushima-Korea Straits, J. Geophys. Res., 107, 3065, doi:10.1029/2000jc000702, 2002.

Isobe, A. and Matsuno, T.: Long-distance nutrient-transport process in the Changjiang river plume on the East China Sea shelf in summer, J. Geophys. Res., 113, C04006, doi:10.1029/2007jc004248, 2008.

Jacobs, S. S., Fairbanks, R. G., and Horibe, Y.: Origin and Evolution of Water Masses Near the Antarctic continental Margin: Evidence from $H_2^{18}O/H_2^{16}O$ Ratios in Seawater, in: Oceanology of the Antarctic Continental Shelf, edited by: Jacobs, S. S., American Geophysical Union, Washington, D. C., 59–85, 1985.

Jain, S. and Lall, U.: Floods in a changing climate: does the past represent the future?, Water Resour. Res., 37, 3193–3250, 2001.

Jiang, T., Su, B., and Hartmann, H.: Temporal and spatial trends of precipitation and river flow in the Yangtze River Basin, 1961–2000, Geomorphology, 85, 143–154, doi:10.1016/j.geomorph.2006.03.015, 2007.

Jiang, T., Zhang, Q., Zhu, D., and Wu, Y.: Yangtze floods and droughts (China) and teleconnections with ENSO activities, Quaternary Int., 144, 29–37, 2006.

Johnson, K., Hu, C., Belshaw, N., and Henderson, G.: Seasonal trace-element and stable-isotope variations in a Chinese speleothem: The potential for high-resolution paleomonsoon reconstruction, Earth Planet. Sci. Lett., 244, 394–407, doi:10.1016/j.epsl.2006.01.064, 2006.

JODC: available at: http://www.jodc.go.jp/index_j.html (last access: 25 March 2014), 2006.

Kao, S. J., Wu, C.-R., Hsin, Y.-C., and Dai, M.: Effects of sea level change on the upstream Kuroshio Current through the Okinawa Trough, Geophys. Res. Lett., 33, L16604, doi:10.1029/2006gl026822, 2006.

Katoh, O., Morinaga, K., and Nakagawa, N.: Current distributions in the southern East China Sea in summer, J. Geophys. Res.-Oceans, 105, 8565–8573, doi:10.1029/1999jc900309, 2000.

Kitani, K.: Low salinity anomaly observed in the East China Sea by research vessel Yoko-maru, Seikai National Fisheries Research Institute, Fisheries Research Agency, 9–11, 1998.

Kubota, Y., Kimoto, K., Tada, R., Oda, H., Yokoyama, Y., and Matsuzaki, H.: Variations of East Asian summer monsoon since the last deglaciation based on Mg / Ca and oxygen isotope of planktic foraminifera in the northern East China Sea, Paleoceanography, 25, PA4205, doi:10.1029/2009pa001891, 2010.

Lan, Y., Ding, Y., Kang, E., Ma, Q., and Zhang, J.: The relationship between ENSO cycle and high and low-flow in the upper Yellow River, J. Geog. Sci., 13, 105–111, 2003.

LeGrande, A. N. and Schmidt, G. A.: Sources of Holocene variability of oxygen isotopes in paleoclimate archives, Clim. Past, 5, 441–455, doi:10.5194/cp-5-441-2009, 2009.

Lie, H.-J., Cho, C.-H., Lee, J.-H., and Lee, S.: Structure and eastward extension of the Changjiang River plume in the East China Sea, J. Geophys. Res., 108, C3, 3077, doi:10.1029/2001jc001194, 2003.

Lin, Y.-S., Wei, K.-Y., Lin, I.-T., Yu, P.-S., Chiang, H.-W., Chen, C.–Y., Shen, C.-C., Mii, H.-S., and Chen, Y.-G.: The Holocene Pulleniatina Minimum Event revisited: Geochemical and faunal evidence from the Okinawa Trough and upper reaches of the Kuroshio current, Mar. Micropaleontol., 59, 153–170, doi:10.1016/j.marmicro.2006.02.003, 2006.

Liu, J., Wang, B., and Yang, J.: Forced and internal modes of variability of the East Asian summer monsoon, Clim. Past, 4, 225–233, doi:10.5194/cp-4-225-2008, 2008.

Maher, B. A. and Thompson, R.: Oxygen isotopes from Chinese caves: records not of monsoon rainfall but of circulation regime, J. Quat. Sci., 27, 615–624, doi:10.1002/jqs.2553, 2012.

East Asian summer monsoon precipitation

Y. Kubota et al.

Title Page

Abstract | Introduction

Conclusions | References

Tables | Figures

|◀ | ▶|

◀ | ▶

Back | Close

Full Screen / Esc

Printer-friendly Version

Interactive Discussion

Mao, H. L., Ren, Y. W., and Wan, G. M.: A preliminary investigation on the application of using T-S diagrams for the quantitative analysis of the watermasses in the shallow water area, Oceanol. Limnol. Sinica, 6, 1–22, 1964.

Morimoto, A., Watanabe, A., Onitsuka, G., Takikawa, T., Moku, M., and Yanagi, T.: Interannual variations in material transport through the eastern channel of the Tsushima/Korea Straits, Prog. Oceanogr., 105, 38–46, doi:10.1016/j.pocean.2012.04.011, 2012.

Moy, C. M., Seltzer, G. O., Rodbell, D. T., and Anderson, D. M.: Variability of El Nino/Southern Oscillation activity at millennial timescales during the Holocene epoch, Nature, 420, 162–165, doi:10.1038/nature01194, 2002.

Oba, T.: Paleoceanographic information obtained by the isotopic measurement of individual foraminiferal specimens, Proceedings of the First International Conference on Asian Marine Geology, Shanghai, 7-10 September 1988, China Ocean Press, Beijing, 1990.

O'Neil, J. R., Clayton, R. N., and Mayeda, T. K.: Oxygen Isotope Fractionation in Divalent Metal Carbonates, The J. Chem. Phys., 51, 5547–5558, doi:10.1063/1.1671982, 1969.

Pausata, F. S. R., Battisti, D. S., Nisancioglu, K. H., and Bitz, C. M.: Chinese stalagmite $[\sigma]^{18}$O controlled by changes in the Indian monsoon during a simulated Heinrich event, Nat. Geosci., 4, 474–480, doi:10.1038/ngeo1169, 2011.

Saito, Y., Katayama, H., Ikehara, K., Kato, Y., Matsumoto, E., Oguri, K., Oda, M., and Yumoto, M.: Transgressive and highstand systems tracts and post-glacial transgression, the East China Sea, Sediment. Geol., 122, 217–230, 1998.

Schmidt, G. A., LeGrande, A. N., and Hoffmann, G.: Water isotope expressions of intrinsic and forced variability in a coupled ocean-atmosphere model, J. Geophys. Res., 112, D10103, doi:10.1029/2006jd007781, 2007.

Shackleton, N.: Attainment of isotopic equilibrium between ocean water and the benthonic foraminifera genus Uvigerina: isotopic changes in the ocean during the last glacial, Centre National de la Recherche Scientifique, Coll. Inter, Paris, France, 219, 203–209, 1974.

Shi, Y., Kong, Z., Wang, S., Tang, L., Wang, F., Yao, T., Zhao, X., Zhang, P., and Shi, S.: Mid-Holocene climates and environments in China, Global Planet. Change, 7, 219–233, 1993.

Steinke, S., Glatz, C., Mohtadi, M., Groeneveld, J., Li, Q., and Jian, Z.: Past dynamics of the East Asian monsoon: No inverse behaviour between the summer and winter monsoon during the Holocene, Global Planet. Change, 78, 170–177, doi:10.1016/j.gloplacha.2011.06.006, 2011.

CPD

10, 1447–1492, 2014

East Asian summer monsoon precipitation

Y. Kubota et al.

Title Page

Abstract | Introduction

Conclusions | References

Tables | Figures

|◄ | ►|

◄ | ►

Back | Close

Full Screen / Esc

Printer-friendly Version

Interactive Discussion

Sun, Y., Oppo, D. W., Xiang, R., Liu, W., and Gao, S.: Last deglaciation in the Okinawa Trough: Subtropical northwest Pacific link to Northern Hemisphere and tropical climate, Paleoceanography, 20, PA4005, doi:10.1029/2004pa001061, 2005.

Takayanagi, K., Hasegawa, T., Kiyomoto, T., Okamura, K., and Nishiuchi, K.: Oceanographic survey by reseach vessel: CK line in the East China Sea, Kaiyo Monthly, 40, 9–13, 2008.

Trenberth, K. E., Branstator, G. W., Karoly, D., Kumar, A., Lau, N.-C., and Ropelewski, C.: Progress during TOGA in understanding and modeling global teleconnections associated with tropical sea surface temperatures, J. Geophys. Res., 103, 14291–14324, 1998.

Uchida, M., Ohkushi, K. I., Kimoto, K., Inagaki, F., Ishimura, T., Tsunogai, U., TuZino, T., and Shibata, Y.: Radiocarbon-based carbon source quantification of anomalous isotopic foraminifera in last glacial sediments in the western North Pacific, Geochem. Geophys. Geosyst., 9, Q04N14, doi:10.1029/2006gc001558, 2008.

Uehara, K., Saito, Y., and Hori, K.: Paleotidal regime in the Changjiang (Yangtze) Estuary, the East China Sea, and the Yellow Sea at 6 ka and 10 ka estimated from a numerical model, Mar. Geol., 183, 179–192, 2002.

Waelbroeck, C., Labeyrie, L., Michel, E., Duplessy, J. C., McManus, J. F., Lambeck, K., Balbon, E., and Labracherie, M.: Sea-level and deep water temperature changes derived from benthic foraminifera isotopic records, Quat. Sci. Rev., 21, 295–305, 2002.

Wang, B., Wu, R., and Fu, X.: Pacific-East Asian Teleconnection: How Does ENSO Affect East Asian Climate?, J. Climate, 13, 1517–1536, 2000.

Wang, B., Yang, J., Zhou, T., and Wang, B.: Interdecadal changes in the major modes of Asian-Australian monsoon variability: Strengthening relationship with ENSO since the late 1970s, J. Climate, 21, 1771–1789, 2008.

Wang, P., Clemens, S., Beaufort, L., Braconnot, P., Ganssen, G., Jian, Z., Kershaw, P., and Sarnthein, M.: Evolution and variability of the Asian monsoon system: state of the art and outstanding issues, Quat. Sci. Rev., 24, 595–629, doi:10.1016/j.quascirev.2004.10.002, 2005.

Wang, S.-L. and Chen, C.-T. A.: Bottom water at the center of the north East China Sea in summer: Remnant winter water, Cont. Shelf Res., 18, 1573–1580, 1998.

Wang, Y. J., Cheng, H., Edwards, R. L., An, Z. S., Wu, J. Y., Shen, C. C., and Dorale, J. A.: A high-resolution absolute-dated late Pleistocene Monsoon record from Hulu Cave, China, Science, 294, 2345–2348, doi:10.1126/science.1064618, 2001.

Back | Close

Full Screen / Esc

Printer-friendly Version

Interactive Discussion

Wang, Y., Cheng, H., Edwards, R. L., He, Y., Kong, X., An, Z., Wu, J., Kelly, M. J., Dykoski, C. A., and Li, X.: The Holocene Asian monsoon: links to solar changes and North Atlantic climate, Science, 308, 854–857, doi:10.1126/science.1106296, 2005.

Wang, Y., Cheng, H., Edwards, R. L., Kong, X., Shao, X., Chen, S., Wu, J., Jiang, X., Wang, X., and An, Z.: Millennial- and orbital-scale changes in the East Asian monsoon over the past 224,000 years, Nature, 451, 1090–1093, doi:10.1038/nature06692, 2008.

Xu, K., Milliman, J. D., and Xu, H.: Temporal trend of precipitation and runoff in major Chinese Rivers since 1951, Global Planet. Change, 73, 219–232, doi:10.1016/j.gloplacha.2010.07.002, 2010.

Yamasaki, M., Murakami, T., Tsuchihashi, M., and Oda, M.: Seasonal variation in living planktic foraminiferal assemblage in the northeastern part of the East China Sea, Fossils, 87, 35–46, 2010.

Yuan, D., Cheng, H., Edwards, R. L., Dykoski, C. A., Kelly, M. J., Zhang, M., Qing, J., Lin, Y., Wang, Y., Wu, J., Dorale, J. A., An, Z., and Cai, Y.: Timing, duration, and transitions of the last interglacial Asian monsoon, Science, 304, 575–578, doi:10.1126/science.1091220, 2004.

Zhang, J., Letolle, R., Martin, J. M., Jusserand, C., and Mouchel, J. M.: Stable oxygen isotope distribution in the Huanghe (Yellow River) and the Changjiang (Yangtze River) estuarine systems, Cont. Shelf Res., 10, 369–384, 1990.

Zhang, L., Liu, Z., Zhang, J., Hong, G. H., Park, Y., and Zhang, H. F.: Reevaluation of mixing among multiple water masses in the shelf: An example from the East China Sea, Cont. Shelf Res., 27, 1969–1979, doi:10.1016/j.csr.2007.04.002, 2007.

Zhang, Q., Liu, C., Xu, C.-y., Xu, Y., and Jiang, T.: Observed trends of annual maximum water level and streamflow during past 130 years in the Yangtze River basin, China, J. Hydrol., 324, 255–265, doi:10.1016/j.jhydrol.2005.09.023, 2006.

Zhang, Q., Xu, C.-Y., Jiang, T., and Wu, Y.: Possible influence of ENSO on annual maximum streamflow of the Yangtze River, China, J. Hydrol., 333, 265–274, doi:10.1016/j.jhydrol.2006.08.010, 2007.

Title Page

Abstract | Introduction

Conclusions | References

Tables | Figures

|◄ | ►|

◄ | ►

Back | Close

Full Screen / Esc

Printer-friendly Version

Interactive Discussion

Table 1. Modern temperature, salinity, and $\delta^{18}O_w$ values for water masses averaged from June to October in a 1° × 1° box noted in the right columns. Data are from monthly mean data statistically processed by Japan Ocean Data Center. $\delta^{18}O_w$ values are converted from salinity values using the present-day relation equation $\delta^{18}O_w = 0.203S - 6.76$ by Oba (1990).

	Temperature (°C)	±	Salinity (PSU)	±	$\delta^{18}O_w$ (‰, VSMOW)	±	Area	Depth (m)
KSW	28.31	0.91	34.23	0.31	0.19	0.06	24–25° N 122–123° E	0
KSSW	23.41	0.82	34.71	0.07	0.29	0.01	24–25° N 122–123° E	100
CDW	23.52	4.02	27.31	1.29	−1.22	0.26	31–32° N 122–123° E	0
TSW	26.83	1.00	33.84	0.014	0.12	3	23–25° N 119–120° E	0–50

Fig. 1. A map showing the Changjiang drainage Basin (Gray shaded area), Datong hydrological station, cave locations of the stalagmite's study, and the core site of KY07-04-01. A dashed gray line represents the modern northern limit of the monsoon front.
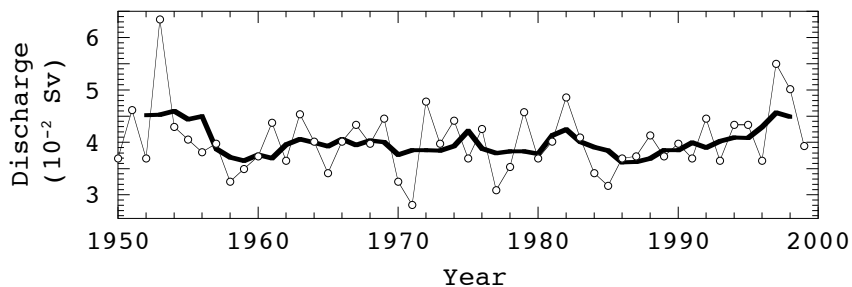
Fig. 2. Wet season (May–October) discharges of the Changjiang River at Datong station from 1950 to 2000. Bold line represent 5-year running mean (data from Fang et al., 2011).

CPD

10, 1447–1492, 2014

East Asian summer
monsoon
precipitation

Y. Kubota et al.

Title Page

Abstract | Introduction

Conclusions | References

Tables | Figures

|◄ | ►|

◄ | ►
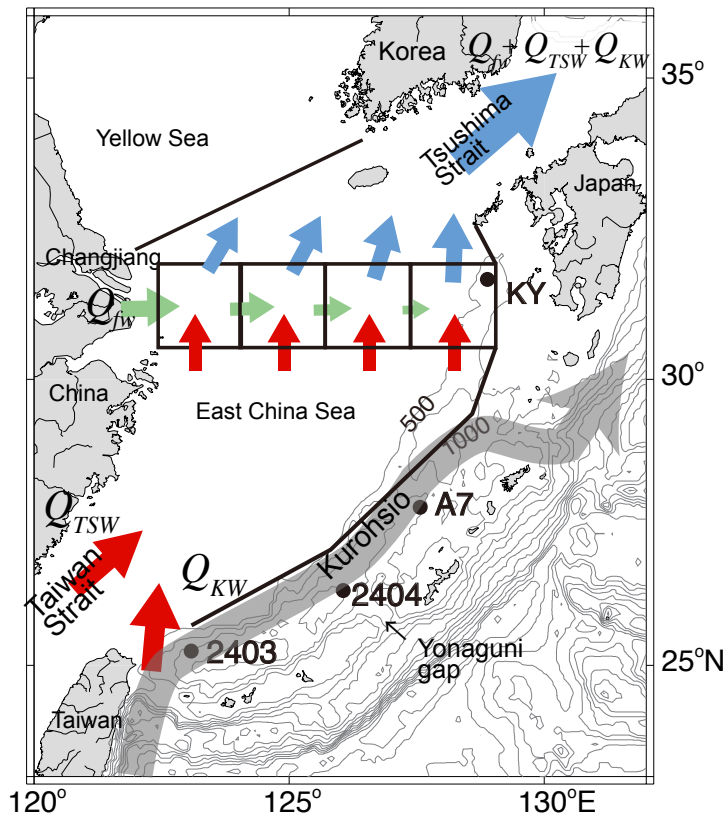
Back | Close

Full Screen / Esc

Printer-friendly Version

Interactive Discussion

Fig. 3. A map showing the simplified modern current system during summer in the East China. Water fluxes into the ECS shelf are described as Q_{KW}, Q_{TSW}, Q_{CFW}. Subscripts KW, TSW, CFW represent Kuroshio Water, Taiwan Strait Water, and Changjiang freshwater, respectively. Red arrows represent fluxes of Kuroshio Water and Taiwan Strait Water onto the shelf. Green arrows represent fluxes of Changjiang freshwater of each box. Blue arrows represent fluxes of seawater mixed with the Changjiang freshwater. Gray arrow represents the Kuroshio Current in the Okinawa Trough. Net water exchange between the Yellow and East China Seas are not taken into account. The Kuroshio Waters are considered to be intruding to the shelf area mainly through the northeastern Taiwan. Sites of KY07-04-01 (this study), A7 (Sun et al., 2005), 2404 (Chen et al., 2010), and 2403 (Lin et al., 2006) are denoted as closed circles.
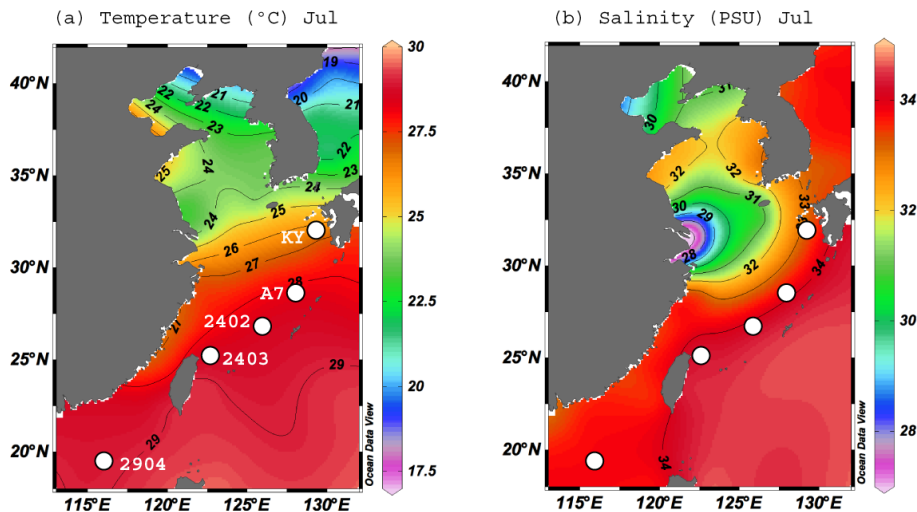
Fig. 4. Sea surface temperature (SST) and sea surface salinity (SSS) **(a)** and **(b)** in July in the ECS (World Ocean Atlas 2009, Locarnini et al., 2010; Antnov et al., 2010) and core locations. Figures made with Ocean Data View (Schlitzer, 2009).
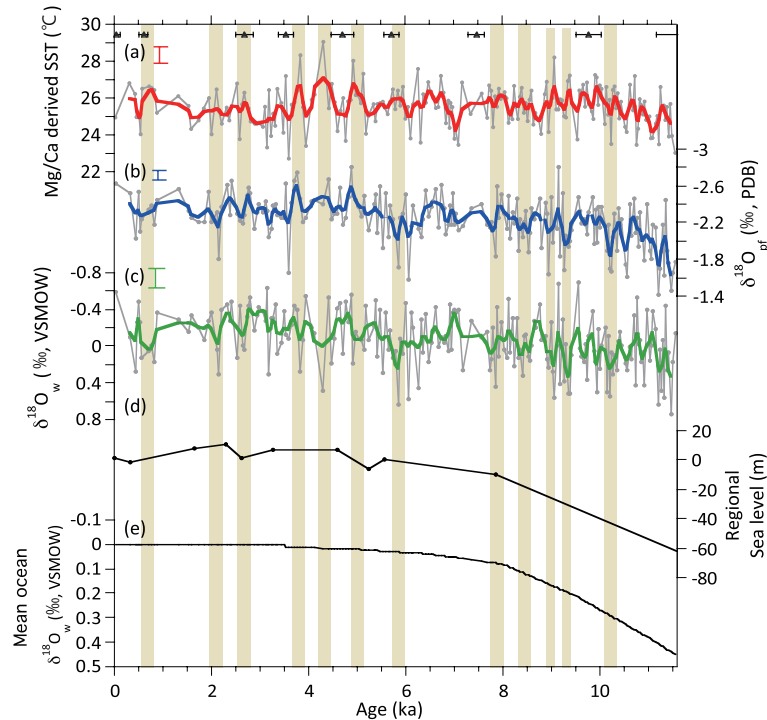
Fig. 5. Results of reconstructions of temporal variations in **(a)** Mg / Ca-derived SST, **(b)** $\delta^{18}O_{pf}$, **(c)** $\delta^{18}O_w$ of KY07-04-01 core. Errors are represented as bars. Bold lines in **(a)** to **(d)** represent 5-points weighted mean of the raw data. **(d)** Time-series of regional sea-level record in the East China Sea (Saito et al., 1998). The bottom figure **(e)** shows temporal changes in global mean ocean $\delta^{18}O_w$ after Waelbroeck et al. (2002). ^{14}C age controlling points of KY core are represented as triangles in upper panel with 2σ errors. Brown bars represent heavier $\delta^{18}O_w$ events of KY.
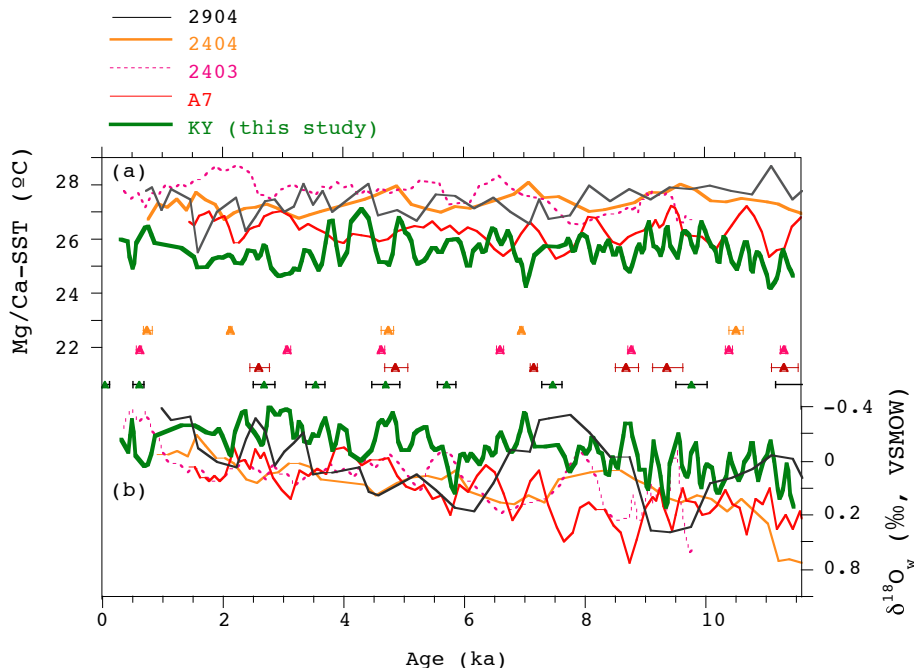
Fig. 6. Diagrams show temporal changes in **(a)** Mg/Ca-derived SST and **(b)** $\delta^{18}O_w$ of four cores in the East China Sea during the Holocene. Core locations are described in Fig. 4. Black, orange, pink dot, and red lines represent 3-point running mean data for cores 2904 (Steinke et al., 2011), 2404 (Chen et al., 2010), 2403 (Lin et al., 2006), and A7 (Sun et al., 2005) cores, respectively. Green represents 5-point running mean for core KY. Triangles and bars in orange, pink, red, and green colors represent age control points for cores 2404, 2403, A7, and KY and errors of 1σ (2904, 2404, and 2403), 2σ (A7 and KY).
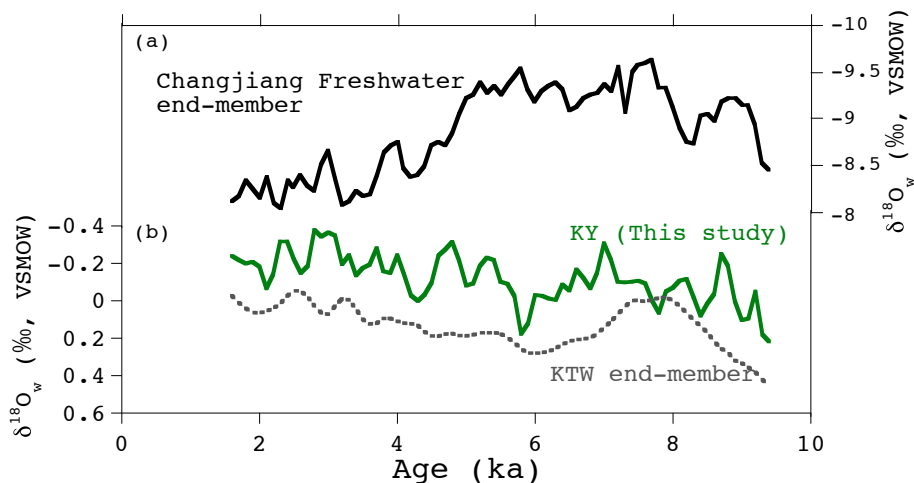
Fig. 7. (a) δ^{18}O of the Changjiang freshwater end-member calculated from a speleothem in Heshang Cave in China (Hu et al., 2008) and original data points are 25-points averaged and linearly interpolated every 100 year interval. **(b)** δ^{18}O$_w$ of the marine cores in the northern ECS (KY07-04-01, in green) and end-member of Kuroshio Taiwan Water (KTW; gray dotted line).
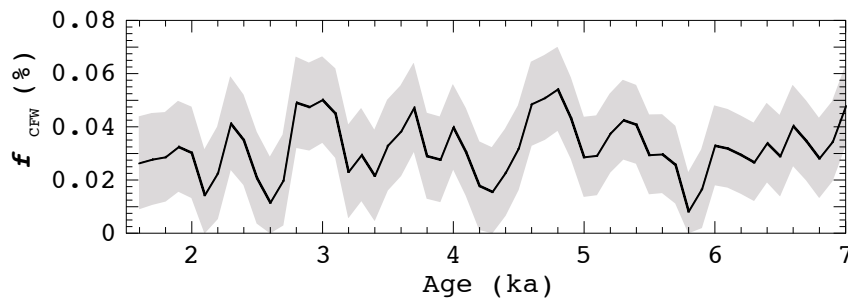
Fig. 8. Relative contribution of the Changjiang freshwater (f_{CFW}) at site KY in the northern ECS. Gray shades indicate uncertainties propagated from 1σ error of $\delta^{18}O_w$ ($1\sigma = \pm 0.14\,‰$) for core KY.

CPD

10, 1447–1492, 2014

East Asian summer monsoon precipitation

Y. Kubota et al.

Title Page

Abstract | Introduction

Conclusions | References

Tables | Figures

|◄ | ►|

◄ | ►
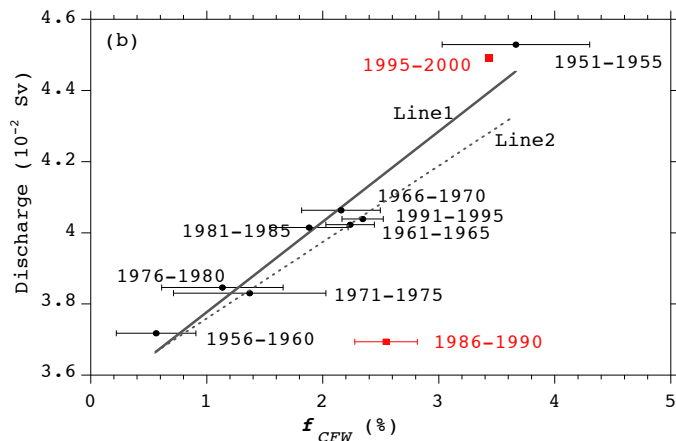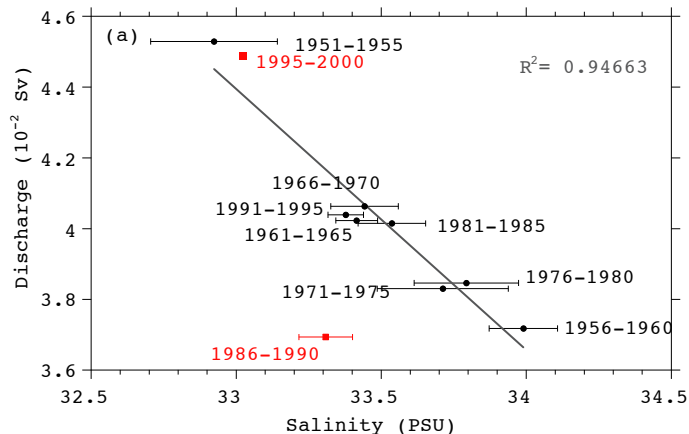
Back | Close

Full Screen / Esc

Printer-friendly Version

Interactive Discussion

Fig. 9. (a) Modern relathionship between 5 year mean salinity (July-August) around site KY and freshwater discharge of the Changjiang. Comparison of 5 year mean wet season (May–October) Changjiang discharge at Datong Station from 1951–1995, showing robust relationship between them. Bars associated with black filled circles represent σ^2 of the annual mean for the 5 year interval. Original salinity data collected by Nansen bottle water sampler, MBT, CTD, and XBT measurements are downloaded within the area of 31–32° N, 128–129° E from online archive (http://www.jodc.go.jp/index_j.html). These salinity data are annually averaged from the depth of 0 to 30 m, and further averaged every 5-year interval from 1951 to 2000. **(b)** Comparison of 5 year mean wet season (May to October) Changjiang discharge at Datong Station with 5 year mean relative contribution of Changjiang freshwater (f_{CFW}) in the northern ECS derived from observational salinity data (31–32° N, 128–129° E). 5 year mean data in time interval from 1986 to 1990 is omitted (symbol of square in red color).

Title Page

Abstract | Introduction

Conclusions | References

Tables | Figures

|◄ | ►|

◄ | ►

Back | Close

Full Screen / Esc

Printer-friendly Version

Interactive Discussion

Discussion Paper | Discussion Paper | Discussion Paper | Discussion Paper

CPD

10, 1447–1492, 2014

East Asian summer monsoon precipitation

Y. Kubota et al.

Title Page

Abstract | Introduction

Conclusions | References

Tables | Figures

I◄ | ►I

◄ | ►

Back | Close

Full Screen / Esc

Printer-friendly Version

Interactive Discussion
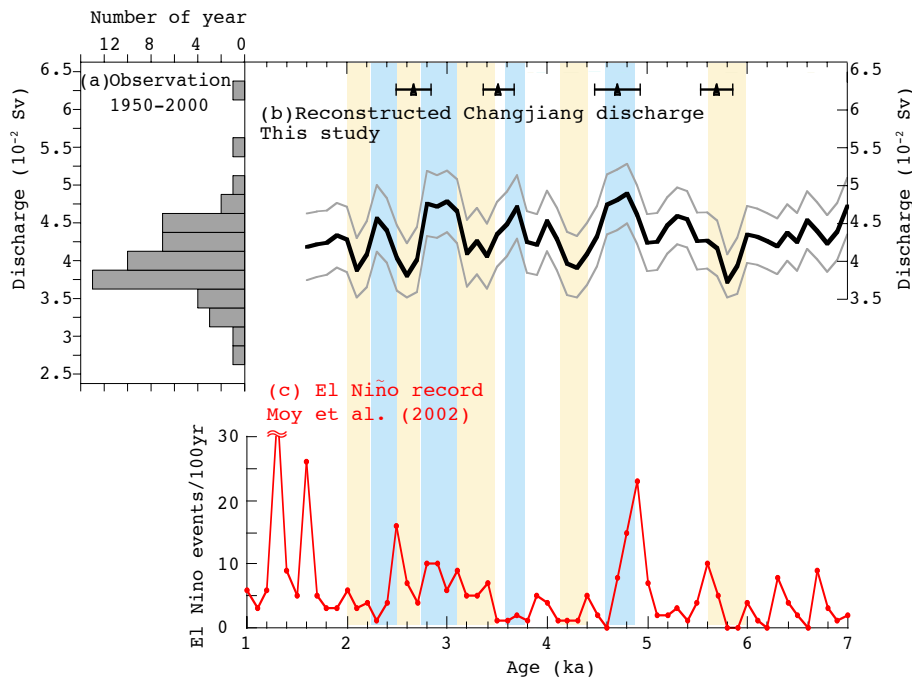
Fig. 10. The upper panels show **(a)** a frequent distribution of the observational Changjiang discharge data during summer (May-October) at Datong Station from 1950–2000 and **(b)** reconstructed Changjiang freshwater discharge (Q_{CFW}) by using core KY $\delta^{18}O_w$ with uncertainties propagated from 1σ error of $\delta^{18}O_w$ ($1\sigma = \pm 0.14\,‰$) for the result of core KY. Brown and blue bars correspond to the time interval when the lower Changjiang discharge events (brown) and higher discharge events (blue). **(b)** The reconstruction of the precipitation (Hu et al., 2008). The lower panel show **(d)** The occurrence of El Niño per 100 yr reconstructed by Moy et al. (2002) using a sediment from lake in Equador.
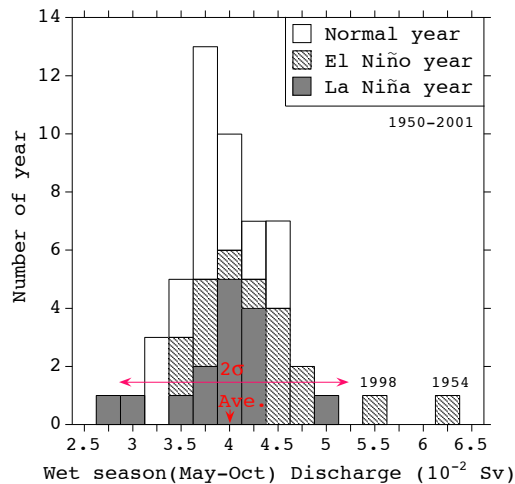
Fig. 11. Modern frequent distribution of the Changjiang discharge during summer (May–October) from 1950 to 2001 at Datong Station shows the relationship to the occurrence of El Niño and La Niña events. The discharge in 1954 and 1998 show extremely high which exceeds 2σ of the standard deviation of the interannual variations from 1950–2001.